Title: Age-related changes in Higuchi's fractal dimension in healthy human EEG are anti-correlated with changes in oscillatory power and 1/f slope

Abbreviated title: Dependence of Higuchi's fractal dimension on oscillations and 1/f slope

Authors: Srishty Aggarwal[1] and Supratim Ray[2*]

Affiliations:

[1]Department of Physics, Indian Institute of Science, Bengaluru, India, 560012,

[2] Centre for Neuroscience, Indian Institute of Science, Bengaluru, India, 560012,

Telephone +91 80 2293 3437, Facsimile +91 80 2360 3323

*** Corresponding author:** sray@iisc.ac.in

Keywords: EEG, Higuchi's fractal dimension, oscillations, aperiodic activity

Declaration of interests: The authors declare no competing financial interests.

Funding disclosure and Acknowledgements: The authors would like to thank Prof. Banibrata Mukhopadhyay for invaluable discussion and suggestions. This work was supported by Tata Trusts Grant and Wellcome Trust/DBT India Alliance (Senior fellowship IA/S/18/2/504003) to SR and Prime Minister Research Fellowship to SA.

Abstract

Non-linear dynamical methods such as Higuchi's fractal dimension (HFD) are often used to study the complexities of brain activity. In human electroencephalogram (EEG), while power in the gamma band (30-70 Hz) and the slope of the power spectral density (PSD) have been shown to reduce with healthy aging, there are conflicting findings regarding how HFD and other measures of complexity vary with aging. Further, the dependence of HFD on features obtained from PSD (such as gamma power and slope) has not been thoroughly probed. To address these issues, we computed time and frequency resolved HFD for EEG data collected from elderly population (N=217), aged between 50-88 years, for baseline (BL) eyes open state and during a fixation task in which visual grating stimuli that induce strong gamma oscillations were presented. During BL, HFD increased with age at frequencies upto 150 Hz, but surprisingly showed an opposite trend at higher frequencies. Interestingly, this change in HFD was opposite to the age-related change in PSD 1/f slope. Further, stimulus-related changes in HFD were anti-correlated with the changes in oscillatory power. However, age classification using HFD was slightly better than classification using spectral features (power and slope). Therefore, HFD could effectively integrate various spectral features as well as some non-linearities not captured using spectral analysis, which could enhance our understanding of brain dynamics underlying healthy aging.

Significance Statement

Higuchi's fractal dimension (HFD) is used widely to understand the complexity and non-linearities in brain signals. Previous studies have found inconsistent results regarding the change of HFD with aging. We tested whether this could be due to changes in spectral measures like oscillatory power and slope with aging by computing time-frequency resolved HFD for EEG data from elderly subjects (N=217; 50-88 years). We found that HFD increased with age upto 150 Hz, but decreased at higher frequencies. Interestingly, age-related changes in HFD were negatively correlated to the corresponding changes in slope and oscillatory power. Age classification using HFD was slightly better than spectral features, suggesting that HFD effectively integrates spectral as well as non-linear changes in brain signals with aging.

Introduction

Aging is associated with a multitude of physical, biological, and cognitive transformations that exert significant impact on overall health and mental well-being. Throughout the transition from mid to late life, the brain undergoes notable age-related alterations in both morphology and physiological dynamics that are intricately intertwined with changes in cognition and behavior (Phillips and Andrés, 2010; Harada et al., 2013). In recent years, there has been a burgeoning interest in non-linear dynamics-based approaches to understand the complexity of brain activity (Anokhin et al., 1996; Drachman, 2006; Rabinovich et al., 2006; Díaz Beltrán et al., 2024). Fractal dimension (FD) has emerged as a powerful tool to probe non-linear changes in the brain, offering valuable insights into various neurological conditions (Raghavendra and Dutt, 2011).

There are a variety of methods used to compute FD, such as box counting dimension, correlation dimension (CD), Katz method and Higuchi's method (Lau et al., 2022). Among these, Higuchi's fractal dimension (HFD) has demonstrated superior accuracy and stability (Higuchi, 1988; Esteller et al., 2001) as a complexity measure, making it particularly useful in different areas of neurophysiology (Werner, 2010). It has been widely employed for sleep physiology, nonionizing radiation, neurobiology, traumatic brain injury, neurodegenerative and neuromodulation studies (Kesić and Spasić, 2016; Olejarczyk et al., 2024). Recently, Smits and colleagues (2016) showed that HFD during resting state varies with age like an inverse parabola – it first increases from young to adulthood (up to 50 years) and then decrease. These results suggest a reduction in complexity with age in elderly population, consistent with another study that used multiscale entropy (McIntosh et al., 2014), but inconsistent with other studies that have shown opposite trends in CD and entropy (Anokhin et al., 1996; Hogan et al., 2012). On the other hand, age related changes in

electroencephalogram (EEG) measured using traditional linear methods like power spectral density (PSD) have shown more consistent trends. For example, oscillatory activity in alpha band (8-12 Hz) has been shown to reduce with aging (Babiloni et al., 2006; Scally et al., 2018). Similarly, slope of the PSD, which could indicate excitation-inhibition (E-I) balance, becomes shallower with age (Voytek et al., 2015). Stimulus-induced narrowband gamma oscillations, which are induced by presenting large visual gratings, also weaken with age (Murty et al., 2020).

Some studies have hinted at potential correlations between FD and oscillatory power (Kronholm et al., 2007; Akar et al., 2015; Stojadinović et al., 2020), but a detailed spectro-temporal comparison has not been done. As the literature on change of spectral measures with age is quite established, such associations between PSD measures and FD could help resolve the conflicting findings regarding the change in FD with age. Also, it could convey whether brain signals have significant non-linearity or are linear measures enough to provide detailed information about brain dynamics.

We, therefore, investigated the impact of visual grating stimuli on HFD and its modulation with age by utilizing EEG data that was previously collected from a large cohort of subjects (N=217) aged between 50-88 years while they viewed large gratings that induced gamma oscillations (Murty et al., 2020). We explored the frequency dependence of HFD and compared these findings with previously reported changes in stimulus-induced power and PSD slope with age (Murty et al., 2020; Aggarwal and Ray, 2023). Finally, we used linear discriminant analysis (LDA) based classifier to compare the performance of HFD versus PSD based measures for classification of the age of the subject (mid-aged versus old) from EEG data.

Materials and Methods

HFD calculation

HFD was calculated using the algorithm proposed by Higuchi (1988). Here, for a time series $X(1), X(2), X(3), \ldots, X(N)$, taken at a regular time interval, we first construct k new time series, X_k^m, as

$$X_k^m : X(m), X(m+k), X(m+2k), \ldots, X\left(m + \left\lfloor \frac{N-m}{k} \right\rfloor k\right)$$

$$(m = 1,2,3, \ldots, k; k = 1,2,3 \ldots k_{max})$$

m and k are both integers and represent the initial time and the interval time respectively. The length $L_m(k)$ of the curve X_k^m, is given by

$$L_m(k) = \frac{1}{k}\left\{\left(\sum_{i=1}^{\left\lfloor \frac{N-m}{k} \right\rfloor} |X(m+ik) - X(m+(i-1)k)|\right)\frac{(N-1)}{\left\lfloor \frac{N-m}{k} \right\rfloor k}\right\}$$

For each k, the length of the curve $L(k)$ is then obtained by averaging the lengths $L_m(k)$, as

$$L(k) = \frac{1}{k}\sum_{m=1}^{k} L_m(k).$$

Finally, HFD is defined as

$$L(k) \sim k^{-HFD}$$

And obtained by computing L(k) over a range of k (from 1 to k_{max}) and subsequently fitting a line through the log (L(k)) versus log (1/k) plot. We computed HFD using the Matlab code (https://in.mathworks.com/matlabcentral/fileexchange/124331-higfracdim).

$L_m(k)$ can be thought of as the total length of the time series when viewed at a "zoom-out" level of k. The division by $\left\lfloor \frac{N-m}{k} \right\rfloor$ is done to compute the average distance between 2 points $X(m+ik)$ and $X(m+(i-1)k)$. Multiplication by $1/k$ normalizes for the average distance between the points of the original real time series, while multiplication by $(N-1)/k$ accounts for the amount of shortening of the time series when the zoom-out level (k) is increased. HFD is therefore a measure of how much the time series length shortens when viewed at a "zoomed out" level.

HFD is best understood while considering a line (say with a slope of m). Average distance between two points separated by k is simply mk. Average "unit length" after dividing by k is simply m, and the total length (after accounting for the shortening of the time series) is therefore m/k. Hence, with increasing k, the total length should decrease as k^{-1}, and hence a line has an HFD of 1.

HFD calculation is equivalent to a scenario where we embed the time series in boxes of various sizes ($1/k$) and compute the variation in the total length of the time series with the box size. A linear curve as HFD of one, but if the curve is more random, "zooming out" reduces the total length by a greater factor (and hence has a higher HFD). If the curve is really "dense" and covers the whole area on a planar graph, zooming out would lead to a reduction in length given by the square of the zooming factor, yielding an HFD of 2.

Synthetic Signals

To understand HFD and decide the optimum value of the parameter k_{max} for present analysis, we first computed HFD for synthetic signals. This included a straight line, a pure

and a noisy sinusoid, and different forms of colored noise that yield fractal signals. A colored noise has power spectrum characterised by $1/f^{\beta}$, where β is the slope of the fractal signal. The slope is 0 for Gaussian noise or white noise. The slope between 1 and 3 defines a general class of temporal variability of fractals that is the fractional Brownian motion (fBm), with 2 as pure Brownian noise (Eke et al., 2000). fBm is a continuous-time Gaussian process $B_H(t)$ characterized by the "Hurst parameter" H (where $0 < H < 1$), such that $B_H(ct)$ is statistically self-similar to $c^H B_H(t)$, for a constant $c > 0$ (Mandelbrot and Van Ness, 1968). H determines the raggedness of the series, with a higher value leading to a smoother series. It is related to FD by FD = 2-H (Orey, 1970; Mandelbrot, 1985; Falconer, 2013). The autocorrelation function $R(\tau)$ of fBm is given by

$$R(\tau) = \frac{1}{2}(|\tau + 1|^{2H} - 2|\tau|^{2H} + |\tau - 1|^{2H}).$$

The PSD of fBm varies as $f^{-(2H+1)}$ (Mandelbrot and Van Ness, 1968; Molz et al., 1997). Thus $\beta = 2H + 1 = 5 - 2\,FD$ (Higuchi, 1990).

While the increments in Brownian Motion $(X(t) = B_H(s + t) - B_H(s))$, for any s, are independent giving rise to Gaussian series, increments for fBm are not. If H < 0.5, then there is negative autocorrelation, i.e. if there is an increasing pattern in the previous steps, then it is likely that the current step will be decreasing whereas if H > 0.5, the autocorrelation is positive, indicating the opposite trend. Thus, H is an important index to predict the variation in time series and is widely used in stock market strategy as well (Matteo et al., 2005). We computed H using generalised Hurst exponent method (Barabási and Vicsek, 1991; Matteo et al., 2005; Mandelbrot, 2013), as described in the supplementary section.

Neural Signals

The experimental setup and data collection have been explained in detail in the previous studies (Murty et al., 2020, 2021; Kumar et al., 2022; Aggarwal and Ray, 2023), which we summarize below.

Dataset

We used the EEG dataset comprising of 236 healthy human subjects (132 males and 104 females), aged 50-88 years (Murty et al., 2020) under Tata Longitudinal Study of Aging who were recruited from the urban communities of Bengaluru, Karnataka, India. They were clinically identified as cognitively healthy by psychiatrists, psychologists and neurologists at National Institute of Mental Health and Neurosciences (NIMHANS), and M.S. Ramaiah Hospital, Bengaluru, using a combination of tests such as Clinical Dementia Rating scale (CDR), Addenbrook's Cognitive Examination-III (ACE-III), and Hindi Mental State Examination (HMSE). 10 subjects were discarded due to noise (See Artifact Rejection subsection below). Another 9 subjects were discarded for whom data was collected using 32 channels, leading to the usable 64-channel data of 217 subjects (119 males and 98 females).

The participants provided informed consent for the study and monetary compensation was given to them. All the procedures undertaken in the study were approved by the Institute Human Ethics Committees of Indian Institute of Science, NIMHANS, and M.S. Ramaiah Hospital, Bengaluru.

Experimental Settings and Behavioural task

EEG data was collected using 64-channel active electrodes (actiCap) with BrainAmp DC EEG acquisition system (Brain Products GMbH). The electrodes were put according to the international 10–10 system, referenced online at FCz. Raw signals were filtered online between 0.016 Hz (first-order filter) and 1 kHz (fifth-order Butterworth filter), sampled at 2.5 kHz, and digitized at 16-bit resolution (0.1 μV/bit). Subjects were requested to sit in a dark room facing a gamma corrected LCD monitor (BenQ XL2411; dimensions: 20.92 × 11.77 inches; resolution: 1280 × 720 pixels; refresh rate: 100 Hz) with their heads supported by a chin rest. The monitor was placed at (mean ± SD) 58 ± 0.7 cm from the subjects (range: 54.9–61.0 cm). Eye position was monitored using Eyelink 1000 (SR Research Ltd), sampled at 500 Hz.

The task was a passive visual fixation task involving the full screen grating stimuli. It consisted of a single session that lasted for ~20 min and was divided in 2–3 blocks with 3–5 min breaks in between according to subjects' comfort. A fixation spot (0.1°) was shown at the centre of the screen during the trial, on which the subjects were instructed to fixate. After an initial blank period of 1000 ms, 2–3 full screen grating stimuli along with the fixation dot were presented for 800 ms with an interstimulus interval of 700 ms using a customized software running on MAC OS. The stimuli were full contrast sinusoidal luminance achromatic gratings with one of 3 spatial frequencies (1, 2, and 4 cycles per degree) and 4 orientations (0°, 45°, 90°, and 135°), chosen pseudorandomly.

Artifact Rejection

We applied a fully automated artifact rejection framework as described in (Murty and Ray, 2022; Aggarwal and Ray, 2023). Eye-blinks or change in eye position outside a 5° fixation window during −0.5 s to 0.75 s from stimulus onset were removed offline, leading to a rejection of 14.6 ± 2.8% (mean ± SD) repeats. All the electrodes with impedance >25 kΩ were rejected. Impedance of final set of electrodes was (mean ± SD) 5.48 ± 1.83 kΩ. In the remaining electrodes, outliers were detected as repeats with deviation from the mean signal in (i) time or (ii) frequency domains by more than 6 standard deviations (SD), and subsequently electrodes with more than 30% outliers were discarded. Further, repeats that were deemed bad in the visual electrodes (P3, P1, P2, PO3, POz, PO4, O1, Oz and O2) or in more than 10% of the other electrodes were considered bad, eventually producing a set of common bad repeats for each subject. Overall, this led to a rejection of (mean ± SD) 15.58 ± 5.48% repeats. Next, we computed slopes for the power spectrum between 56 Hz and 84 Hz for each unipolar electrode and rejected electrodes whose slopes were less than 0, i.e., power spectrum was tilted upwards.

After removing bad electrodes and common bad repeats using the above criteria, we computed the root mean square value (RMS) of the time series for all the remaining trials for each electrode and declared repeats having RMS values lower than 1.25 µV or higher than 35 µV as new outliers. We then rejected the electrodes that had more than 30% new outliers. Further, any new outlier if it belonged to the visual electrodes or was common in more than 10% of other electrodes was considered a bad repeat and appended to the existing list of bad repeats. After discarding bad electrodes and repeats, 50.43 ±9.92 electrodes and 284.40 ± 88.16 repeats per subject were used for final analysis.

We further discarded the blocks which did not have at least a single good unipolar electrode in the left visual anterolateral (P3, P1, PO3, O1), right visual anterolateral (P2, P4, PO4, O2)

and posteromedial (POz, Oz) electrode groups. We then pooled data across all good blocks for every subject separately for final analysis. This led to a rejection of 10 subjects who did not have any analyzable block.

EEG Data Analysis

All data analyses were done using custom codes written in MATLAB (MathWorks. Inc; RRID:SCR_001622). The analyses were performed using unipolar reference scheme (i.e., all signals referenced to a single electrode, FCz, which was how the data was originally recorded). Similar to the previous studies (Murty et al., 2020, 2021; Kumar et al., 2022; Aggarwal and Ray, 2023), we divided the subjects into two groups: 50–64 years (mid; N=90) and >64 years (old; N=127). We used -500 to 0 ms before and 250 to 750 ms period after the stimulus onset as the "baseline (BL)" and "stimulus (ST)" periods, respectively. The signals between different frequency ranges were obtained by using an infinite filter response fourth order Chebyshev type I band pass filter with bandpass ripple of 0.2 Hz. They were also filtered for the line noise at 50 Hz and its harmonics within ± 2 Hz using the infinite filter response fourth order Chebyshev type I band stop filter.

HFD analysis

For EEG data, HFD was obtained for each trial for BL and ST time series with 1250 data points and then averaged across trials for each electrode. The time-frequency HFD plots were generated using the non-overlapping 0.1 s time window between -0.25 and 1.15 s and 12 Hz frequency window between 1 to 109 Hz.

HFD is dependent on k_{max}. Values of k_{max} between 6-10 have been shown appropriate for HFD computation (Accardo et al., 1997; Spasić et al., 2005). We chose k_{max}= 10 for low frequency signals (<100 Hz), since the log (L) vs log (1/k) curve was linear over this range.

However, at higher frequencies, the log (L) vs log (1/k) curve became non-linear for k_{max}= 10. So, to maintain uniformity, we chose k_{max}= 5 while analysing the frequency dependence of HFD.

Power and Slope Analysis

We obtained power spectrum and time-frequency power spectrogram using the multi-taper method with a single taper using the Chronux Toolbox ((Bokil et al., 2010), RRID:SCR_005547) for individual trials and then averaged across the trials for each electrode. The spectrograms were obtained using a moving window of size 0.25 s and a step size of 0.025 s, yielding a frequency resolution of 4 Hz.

We computed the slope of the 1/f aperiodic component of the trial-averaged PSD for each electrode using the matlab wrapper for Fitting Oscillations and One Over f (FOOOF) toolbox (Donoghue et al., 2020). Similar to (Aggarwal and Ray, 2023), the settings chosen for FOOOF model parameters were: peak width limits: [4 8]; maximum number of peaks: 5; minimum peak height: 0.2; peak threshold: 2.0; and aperiodic mode: 'fixed'. Slopes were computed in frequency ranges from 4 to 350 Hz in steps of 20 Hz with centre frequency between 40 Hz and 300 Hz, having the frequency width of 100 Hz. To avoid poor fitting, we declared ± 4 Hz around the peaks corresponding to the line noise at 50 Hz and its harmonics as "noise peaks" and avoided them for which these noise peaks lay near the end points of frequency range to fit. For the same reason, we discarded slopes less than 0.01 from further analysis.

The correlation coefficients (ρ) and p-value for the change in HFD vs the change in power and slope were obtained using the Matlab command *corrcoef*. We used *fitlm* function in

Matlab that generates the model parameters: $\beta 1$, $\beta 2$ corresponding to $y = \beta 1 + \beta 2 * x$, to obtain the regression line.

Power matching

To remove the dependence of band power change on HFD, we followed the method as described in (Churchland et al., 2010; Kumar and Ray, 2023). We sub-selected subjects from each group such that change in band power had the same distribution within the groups. For this, we first computed the distribution of subjects with respect to the power in each group. Then, we matched the number of subjects from each group within each power bin by randomly selecting subjects from the group with more subjects, to match the subjects in the other group. Ultimately, the subjects in each bin were adjusted to arrive at the common distribution for the two age groups. As each iteration produced a different subset of subjects, the above procedure was repeated 10 times to obtain average value of HFD for the power matched groups.

Classifier analysis

We predicted the age group (mid or old) using a classifier based on linear discriminant analysis (LDA). Both spectral and HFD measures were considered as distinct features. We assessed the classifier performance on the features through the area under the receiver operating characteristic (ROC) curve (AUC) on 5-fold cross-validation sets, where the ROC curve represents the true positive rate against false positive rate. We used the Matlab command *fitdiscr* to generate the LDA based classifier model and then *perfcurve* to compute AUC for the features.

Electrode Grouping

Scalp maps were generated using the topoplot function of EEGLAB toolbox ((Delorme and Makeig, 2004), RRID:SCR_007292) with standard *Acticap 64* unipolar montage of the channels. All the electrodes were divided into 5 groups as occipital (O; O1, Oz, O2, PO3, PO4, PO7, PO8, PO9, PO10, POz), centro-parietal (CP; CP1, CP2, CP3, CP4, CP5, CP6, CPz, P1, P2, P3, P4, P5, P6, P7, P8, Pz), fronto-central (FC; FC1, FC2, FC3, FC4, FC5, FC6, C1, C2, C3, C4, C5, C6, Cz), frontal (F; Fp1, Fp2, F1, F2, F3, F4, F5, F6, F7, F8, Fz, AF3, AF4, AF7, AF8) and temporal (T; T7, T8, TP7, TP8, TP9, TP10, FT7, FT8, FT9, FT10). FCz and Fpz were used as the reference and the ground respectively. To observe the stimulus effect, a subgroup of occipital and centro-parietal electrodes (P3, P1, P2, PO3, POz, PO4, O1, Oz and O2) were chosen, in which strong stimulus-induced gamma was observed and termed as high priority electrodes (HP) (Murty et al., 2020).

Statistical Analysis

Wilcoxon signed rank test was used to compare HFD and H between BL and ST across all trials and all subjects. Kruskal-Wallis (K-W) test and Wilcoxon rank sum (WRS) test were used to compare the medians for power, slope and HFD across groups, as done in previous studies (Murty et al., 2020; Aggarwal and Ray, 2023). The standard error of median (SEM) was computed after bootstrapping over 10,000 iterations.

Data and Code Availability

All spectral analyses were performed using Chronux toolbox (version 2.10), available at http://chronux.org. Slopes were obtained using matlab wrapper for FOOOF

(https://github.com/fooof-tools/fooof_mat). The codes for HFD were taken from https://in.mathworks.com/matlabcentral/fileexchange/124331-higfracdim. The violin plots are plotted using the 'gramm data visualization toolbox' (Morel, 2018). The codes for generating figures in the present work are available at https://github.com/4srihy/TLSAEEGProjectPrograms/tree/master/HFD_AgeProjectCodes. Raw data is freely available at https://osf.io/ebryn/.

Results

To illustrate HFD, we first generated synthetic signals with 1000 data points with known properties and computed their HFD (with $k_{max} = 10$, see Methods for details), as depicted in Fig. 1A. To compare the slope of log (L) vs log (1/k) curve, we changed the offset for each condition such that all traces had the same value of log (L) at k = 1 (or log (1/k) = 0; right panel of Fig. 1A). Each condition was simulated 10 times and mean and SD were computed.

For a straight line (brown trace), the HFD was (mean $\pm$ SD) 1.00 ± 0.00, as expected (see Methods for details). Even for a pure sinusoid (frequency of 10 Hz), HFD remained close to 1 (1.00 ± 0.00), with the log (L) vs log (1/k) plot overlapping with the straight line condition. Since HFD depends on the roughness in the curves, it is ~1 for all straight lines and low frequency pure sinusoids. However, if the frequency of the sinusoid is not much less than the sampling frequency, log (L) vs log (1/k) curve no longer remains linear with 1/k, and a smaller k_{max} than the present one has to be chosen to evaluate HFD. Adding 40% Gaussian noise to the sinusoid (light green trace) increased HFD to 1.84 ± 0.01. For colored noise with β of 1.7 (dark green trace), HFD and H were 1.67 ± 0.02 and 0.36 ± 0.03, consistent with the theoretical values of FD and H of 1.65 and 0.35. Similarly, HFD and β (calculated for the full frequency range circumscribing the power spectrum) were 1.69 ± 0.02 and 1.38 ± 0.06 for fBm with H parameter set to 0.3 (blue trace), consistent with the theoretical results for FD and β as 1.3 and 2.4 respectively. For Gaussian noise covering nearly the full graph (violet trace), HFD was 2.00 ± 0.01.

Next, we examined EEG data for 217 healthy adults aged between 50 and 88 years, grouped as mid (50-64 years; N=90) and old (>64 years; N=127). Subjects performed a fixation task in which full-screen gratings were presented for 800 ms with an inter-stimulus interval of 700 ms. We considered -500 to 0 ms before and 250 to 750 ms periods after stimulus onset as

baseline (BL) and stimulus (ST) periods respectively and computed HFD. We filtered the EEG signals in different frequency ranges using an infinite filter response fourth order Chebyshev type I band pass filter with bandpass ripple of 0.2 Hz. Further, to remove the line noise at 50 Hz and its harmonics, we filtered the signals at corresponding frequencies within ± 2 Hz using the infinite filter response fourth order Chebyshev type I band stop filter.

Stimulus presentation reduced HFD

We first probed the effect of stimulus on HFD. Figure 1B illustrates the process of computation of HFD for a single trial for Oz electrode for one subject. We took the raw time series and filtered it between 1-90 Hz (Fig. 1B, left panel). We computed the HFD for the BL (-0.5 to 0 s) and ST (0.25 to 0.75 s) segments, as highlighted in Fig. 1B left panel, as slopes of log (L) vs log (1/k) curves, shown in Fig. 1B right panel. The curve for BL was slightly steeper than for ST, leading to lower HFD for ST than BL, though the difference was quite small. However, this difference was consistent across trials, as shown in Fig. 1C left panel. The median HFD difference between ST and BL for all trials (n = 139) for a single block was significantly lower than 0 (p = 0.007, Wilcoxon signed rank test), as depicted in Fig. 1C right panel. Across the population, although the HFD values varied considerably, the reduction between BL and ST was consistent, such that the difference was highly significant (Fig. 1D; $p = 5.1 \times 10^{-11}$, Wilcoxon signed rank test).

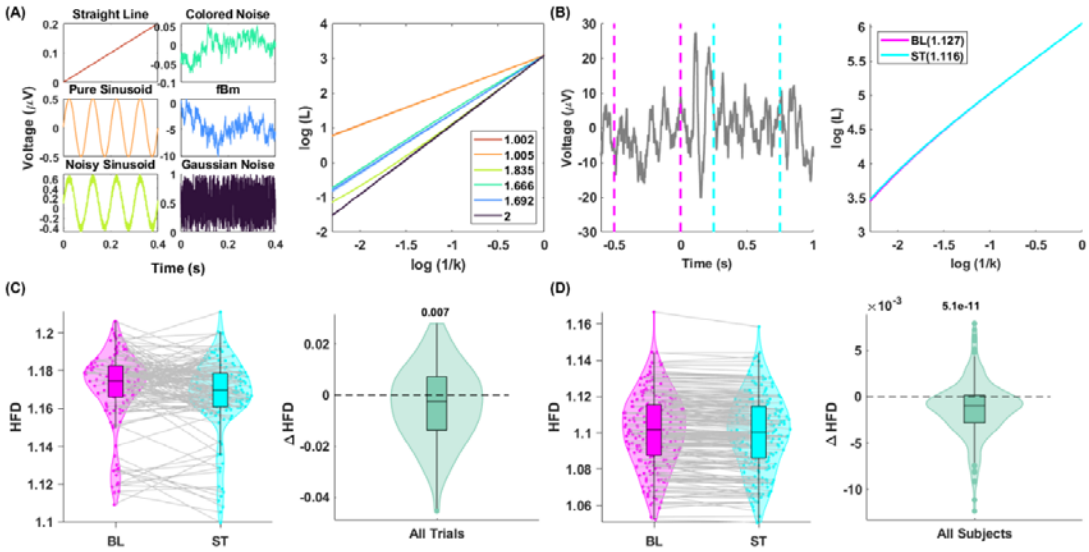

Fig. 1 (A) Different synthetic signals (left panel: straight line of slope 0.5 (brown); sine wave of frequency 10 Hz (orange); sine wave with 40% Gaussian noise added (light green); colored noise with slope (β) of 1.7 (dark green); fractional Brownian motion (fBm) with Hurst index (H) of 0.3 (blue) and Gaussian noise (violet)) and corresponding average log (L) vs log (1/k) curves (right panel). The shaded region around the curves shows $\pm$SD, computed by running the simulations 10 times. The legend shows the average HFD for these signals. **(B)** Time series for one trial for one subject for electrode Oz, filtered between 1 to 90 Hz (left panel). Magenta and cyan vertical lines indicate the BL and ST periods, respectively. Log (L) vs log (1/k) curves for the filtered BL and ST segments with $k_{max} = 10$ (right panel). The HFD (slope of the curves) values are indicated in the legend. **(C)** Violin plots with matched pairs showing the distribution of HFD for BL and ST (left panel) and ΔHFD (right panel) for all trials (n = 139) for electrode Oz. The p-value for median computed from Wilcoxon signed rank test is indicated on the top in the right panel. **(D)** Violin plots showing the distribution of HFD for BL and ST (left panel) and ΔHFD (right panel) for all subjects (N=217).

To cross-verify the HFD computation and the choice of k_{max}, we also checked the effect of stimulus on H (Supplementary Fig. 1). Though H is theoretically related to FD as FD = 2-H (Orey, 1970; Mandelbrot, 1985; Falconer, 2013), for real signals, the relation may not be satisfied (Amezquita-Sanchez et al., 2019). We found that H increased with stimulus, thus, showing an opposite trend of HFD. Moreover, the sum of HFD and H tended to 2 (1.985 ± 0.001 for both BL and ST), which to our knowledge has not been observed for real EEG signals. This essentially validates the choice of $k_{\max}$ and use of HFD as the intrinsic fractal dimension of the signals.

HFD increased with age

Next, we divided EEG electrodes into 5 groups (see Methods for details) and computed HFD for BL and ST periods. Subjects were divided into mid (50-64 years) and old (≥65 years) age groups. For BL, HFD was significantly higher for old group than mid in all electrode groups (p-values shown in the plot, WRS test) as shown in Fig. 2A violin plot and topoplots. While HFD was higher in central electrodes than occipital electrodes for both age groups (Fig. 2A left and centre topoplots), the difference in HFD was higher in occipital electrodes and gradually decreased towards the frontal region, as depicted in Fig. 2A right topoplot (old-mid). The similar difference was observed for ST period (Fig. 2B). However, the change in HFD between ST and BL was more negative in mid group as compared to the old group mainly in occipital (p=0.005, WRS test) and centro-parietal regions (p = 0.002, WRS test; Fig. 2C). This was expected, since the visual stimulus mainly changed the activity in the occipital and other nearby electrodes. Therefore, we have presented further results for a subgroup of these electrodes, termed “high-priority” (HP) electrodes here and in previous studies, highlighted in Fig. 2A left topoplot.

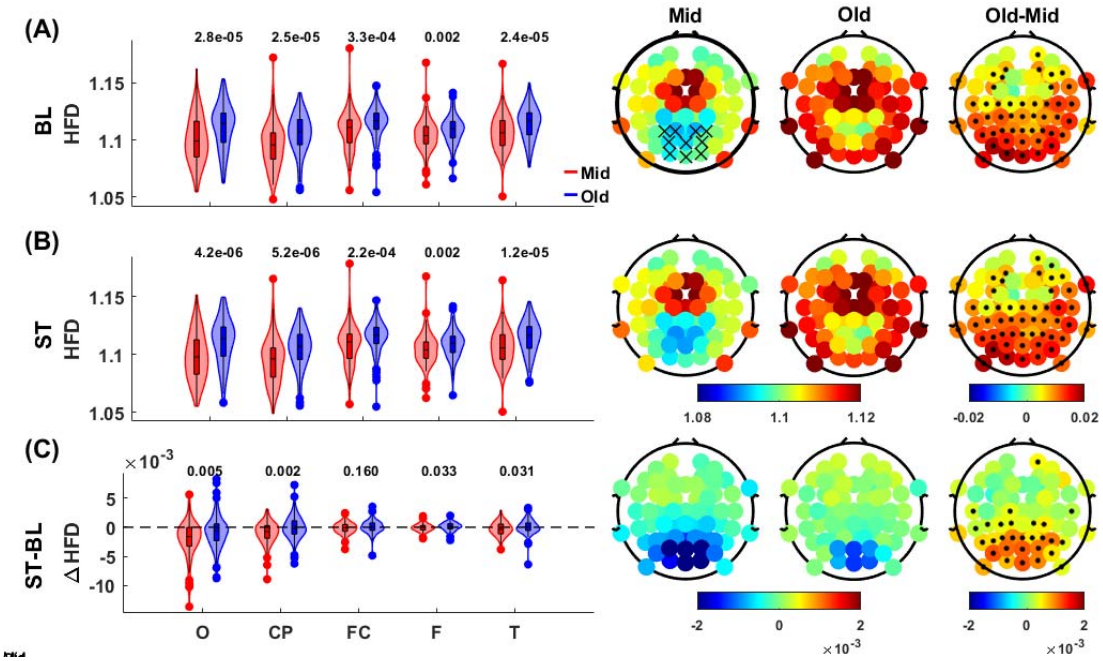

Fig. 2 (A) (Left) Violin plots showing the comparison of HFD for BL in mid and old aged group for different electrode groups. The p-values, computed from Wilcoxon rank sum (WRS) test are indicated at the top of the distribution for the corresponding electrode group. (Right) Topoplots showing the median HFD across the electrodes for mid (left), old (center) and difference: old-mid (right). 'x' in the left topoplot indicate high-priority (HP) electrodes. Electrodes with significant difference ($p < 0.05$, WRS test) are highlighted in black in the right topoplot. Similar comparison is shown for ST in **(B)** and Diff (ST-BL) in **(C)**.

HFD increased with frequency

As shown in previous studies, the visual stimuli induced strong stimulus-induced gamma oscillations that weakened with age (Murty et al., 2020). To test whether changes in HFD were related to the changes in the power spectrum of the signals, we computed HFD as a function of frequency of the signal. Figure 3A shows the BL segment of the signal (the full signal is shown in the inset) for a single trial for Oz electrode for one subject. We then

filtered the signal in different frequency ranges as indicated in Fig. 3B using an infinite filter response fourth order Chebyshev type I band pass filter with bandpass ripple of 0.2 Hz. We chose these ranges to avoid the line noise and its harmonics. The corresponding log (L) vs log (1/k) curves up to $k_{max} = 10$ with dotted lines are shown in Fig. 3C. As the frequency range increased, the log (L) curve became more non-linear. To maintain uniformity for choosing linear range for log (L) vs log (1/k), we computed HFD for all frequency ranges up to $k_{max} = 5$, as indicated by solid lines in Fig. 3C. Figure 3D shows the variation of the HFD with centre frequency for the frequency ranges shown in Fig. 3B. As expected, HFD increased with frequency since higher frequency range signals were less smooth. We further calculated the HFD for shorter segments of the signal to generate the time-frequency (TF) HFD profile. Figure 3E depicts this profile for all trials (n = 139) for HP electrode group for one subject. The corresponding delta TF plot in Fig. 3F, obtained after subtracting the mean BL HFD values at each frequency, showed a strong reduction in HFD from 1 to 40 Hz during the transient period (0 to 0.25 s) and a steady decrease around ~20 Hz during the ST period. As shown later, this reduction in HFD after stimulus onset matches with the increase in oscillatory power in the slow gamma range after stimulus onset.

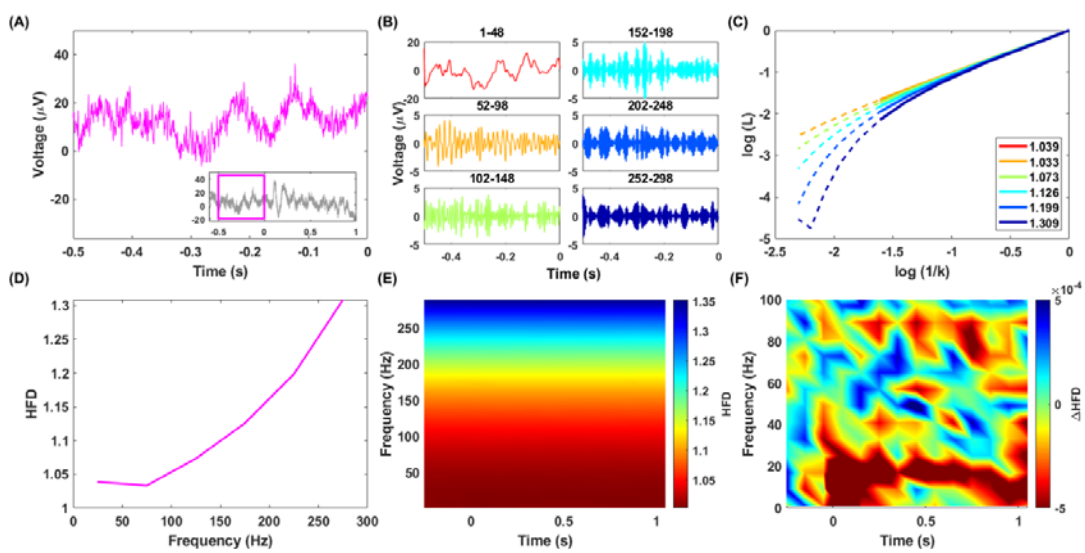

Fig. 3 (A) BL time series for a single trial for Oz, segmented from the whole time series as shown in the inset with the box highlighting the BL period. **(B)** BL time series filtered in different frequency ranges. **(C)** Corresponding log (L) vs log (1/k) curves for $k_{max} = 10$ (dotted) and $k_{max} = 5$ (solid). The HFD computed with $k_{max} = 5$ are indicated in legends in (C) and are plotted with respect to centre frequency in **(D). (E)** Time-frequency (TF) plot for HFD averaged across all trials (n = 139) for HP electrode group. **(F)** Corresponding delta TF plot showing the change in HFD during stimulus and transient periods with respect to baseline.

Change in frequency dependant HFD with age during baseline was opposite to the change in the slope of the PSD

Next, we explored the changes in HFD with age as a function of frequency. We computed HFD (with $k_{max} = 5$) for signal in the BL period after filtering with centre frequencies from 40 Hz to 300 Hz (in steps of 10 Hz) by taking ± 50 Hz around each centre frequency (for center frequencies of 40 and 50 Hz, the lower limit was set to 4 Hz). Figure 4A left panel shows the HFD as a function of frequency in HP electrode group for mid and old age groups. Although the difference of HFD between these groups was small, the curves were significantly different at many frequency ranges, as indicated by black ($p<0.05$; K-W test) and green ($p<0.01$; K-W test) bars. The change in HFD (old-mid) is shown in Fig. 4A right panel. Interestingly, the age-dependant increase in HFD during BL, as shown in Fig. 2A was present only up to ~150 Hz. At higher frequencies, HFD was lower for old group as compared to mid group.

To probe the dependence of HFD on spectral measures, we compared the age-related BL HFD changes with the similar changes in power and slope. We plotted the BL PSD for mid

and old groups (Fig. 4B top left panel) with frequency resolution 2 Hz and the change in power in dB (obtained by subtracting log power of mid from log power of old and then multiplying by 10; Fig. 4B top right panel). We also plotted the slope and the corresponding change with age (old-mid) computed between the frequency ranges from 4 to 350 Hz in steps of 20 Hz with centre frequency between 40 Hz and 300 Hz and the frequency width of 100 Hz. While old group had lower power at frequencies till ~50 Hz and higher power beyond (Fig. 4B top panel), slope was lower for old-aged group up to ~150 Hz and then was higher (Fig. 4B bottom panel), as reported previously (Aggarwal and Ray, 2023). The trend of the HFD change seemed opposite to the age dependant slope change but not much on the change in power.

To better quantify these changes, we plotted HFD with power and slope for the two age groups and corresponding ΔHFD with ΔPower and ΔSlope. Here power is computed by summing the PSD for frequency ranges obtained at the centre frequencies between 40 and 300 Hz in the steps of 20 Hz with the frequency width of 100 Hz. Figure 4C top panel shows the dependence of HFD on power for mid and old (left) and the change in power (in dB) versus the change in HFD between the groups (right). As HFD increased with frequency due to the increase in roughness of signal and power decreased with frequency, HFD and power were anti-correlated. There was a significant negative correlation between ΔHFD and ΔPower (correlation coefficient (ρ) = -0.69, p = 0.006). On the other hand, while HFD did not show a specific relationship with slope as depicted in Fig. 4C bottom left panel, ΔHFD showed a surprisingly strong negative correlation with ΔSlope with age (Fig. 4C bottom right panel; ρ = -0.98, $p = 5.1 \times 10^{-10}$). This anti-correlation between ΔHFD and ΔSlope persisted even if k_{max} was not kept the same for all frequency ranges (data not shown). Thus, the change in the HFD in aging as a function of frequency strongly reflected the corresponding changes in

PSD slope, indicating that HFD depends more on the rate of change of power with frequency than the magnitude of change of power itself.

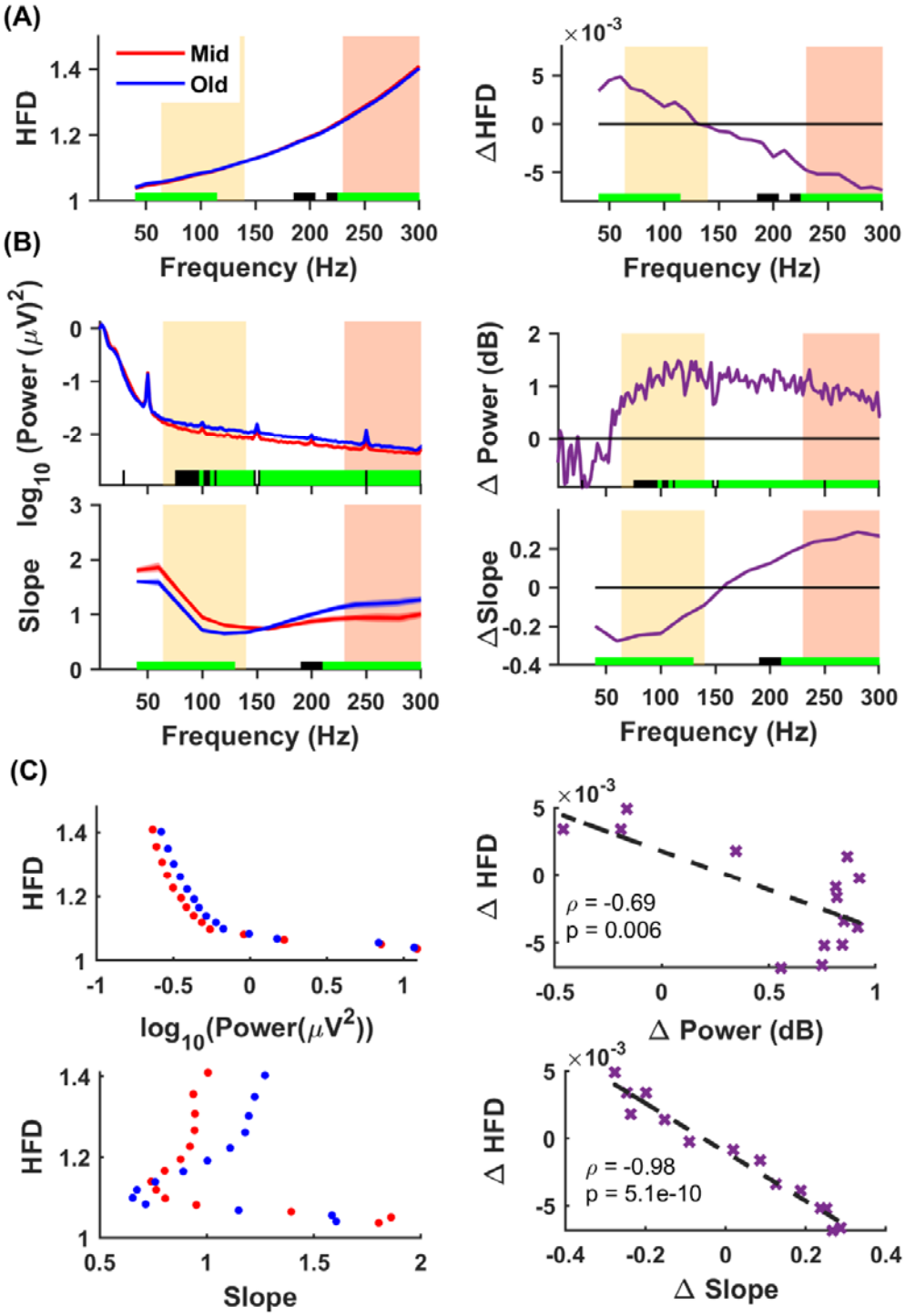

Fig. 4 (A) HFD, **(B) (Top)** Power spectral density (PSD), **(bottom)** Slope versus frequency for BL period in HP electrodes for mid and old groups (left) and their corresponding difference (old-mid; right). In the left panels, solid traces represent the median and shaded region around them indicates ±SEM across subjects, computed after bootstrapping over 10,000 iterations. Coloured bars at the abscissa at the bottom represent significance of differences between mid and old (black: $p < 0.05$ and green: $p < 0.01$, Kruskal-Wallis (K-W) test). Yellow and orange boxes represent the low frequency range (LFR; 64-140 Hz) and the high frequency range (HFR; 230-300 Hz) respectively. In the right panels, violet traces represent the difference of median of old and mid group shown in the left panels and coloured bars at the abscissa are same as the left ones. **(C) (Left)** HFD versus power (top) and slope (bottom) at the centre frequencies between 40-300 Hz in steps of 20 Hz and frequency width of 100 Hz (left) for mid and old. **(Right)** The corresponding group difference of ΔHFD vs ΔPower (top) and ΔSlope (bottom) respectively. 'x' represents the data points and the regression line is in black. The correlation coefficient (ρ) and p-value are indicated in each subplot.

Change in frequency dependant HFD with age during stimulus was opposite to the change in Power

To probe age-related effect of ST on HFD and its dependence on gamma power, we first compared the ΔPower between the two age groups with respect to frequency (Fig. 5A top panel). While there was no significant power difference in the alpha range (8-12 Hz; pink band), mid-aged group had significantly higher power than old group in both slow (purple, 20-34 Hz) and fast (grey, 36-66 Hz; $p < 0.05$: black and <0.01: green, K-W test). The same was visible in TF spectra for change in power obtained by subtracting average BL power

from the raw power in Fig. 4B top panel for mid (left), old (centre) and old-mid (right), as shown previously (Murty et al., 2020). To compare corresponding changes in HFD, we computed ΔHFD (ST-BL) for continuous non-overlapping frequency ranges with centre frequencies lying between 7 and 103 Hz and frequency width of 12 Hz (Figure 5A, bottom plot), and for non-overlapping 0.1 s time window between -0.25 and 1.15 s and frequency width of 12 Hz for TF HFD plots (Fig 5B bottom panels). While ΔHFD with respect to stimulus was higher in alpha range, it showed a reduction in gamma bands. In the alpha band, ΔHFD was not different between the two age groups. However, ΔHFD was significantly more negative in mid-aged group than old in slow and fast gamma bands (colorbars of the TF plot for ΔHFD are reversed compared to ΔPower to observe this similarity). Fig. 5B top and bottom panels look visually similar, indicating that the ΔHFD is negatively related to ΔPower.

To test whether the change in HFD with age could be explained by corresponding changes in the oscillatory components of PSDs, we sub-selected the subjects from each group such that they had same distribution of power in specific bands ((Kumar and Ray, 2023); See Materials and Methods). When we matched subjects for alpha (8-12 Hz), slow gamma (20-34 Hz) and fast gamma power (36-66 Hz) respectively, the corresponding difference of ΔHFD in those frequency ranges became non-significant (Fig. 6), while the difference in other frequency band remained similar to the non-matched criterion. This indicated a strong dependence of HFD on oscillatory power.

The frequency dependence of HFD on slope and power suggests that for signals filtered between 1-90 Hz, the increase in HFD with age in BL was dominated by the effect of slope in the frequency range 60-90 Hz and the decrease in HFD during ST with respect to BL was due to the increase in power in gamma band (Fig. 2).

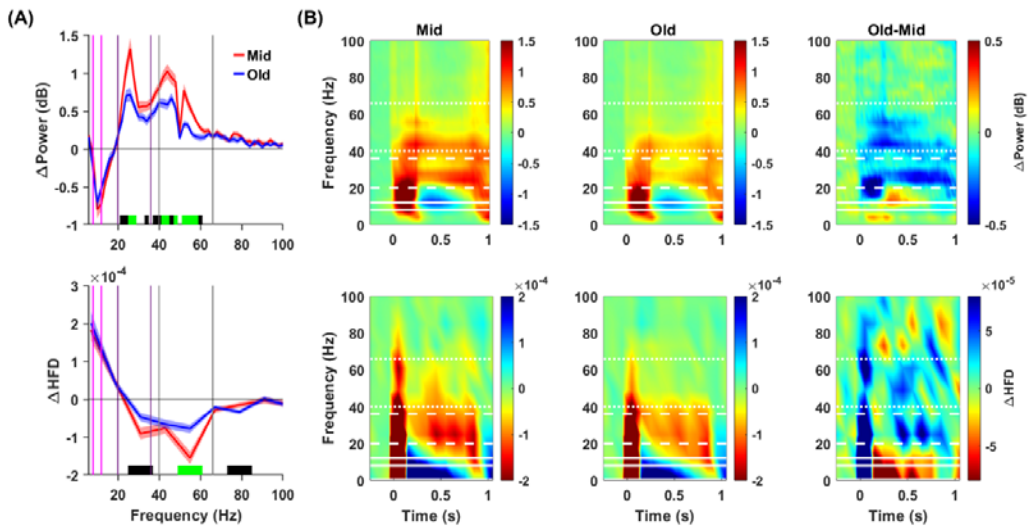

Fig. 5 (A) Change in power in dB (top) and HFD (bottom) during the ST with respect to the BL for the two age groups. Solid traces represent the median and shaded region around them indicates ±SEM across subjects, computed after bootstrapping over 10,000 iterations. Coloured bars at the abscissa in the bottom panel represent significance of differences of slopes between mid and old (black: $p < 0.05$ and green: $p < 0.01$, K-W test). The pink, purple and grey vertical lines represent alpha (8-12 Hz), slow-gamma (20-34 Hz) and fast-gamma (36-66 Hz) frequency bands respectively. **(B)** Delta TF plots for change in power (top) and HFD (bottom) for mid (left), old (centre) and difference (old-mid; right).

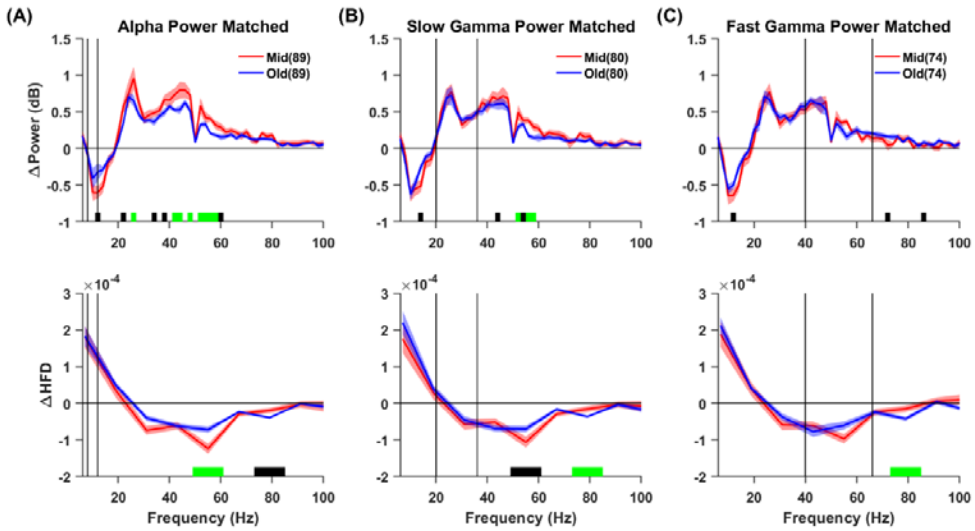

Fig. 6 Change in power (top) and the change in HFD (bottom) for power matched subjects in **(A)** alpha, **(B)** slow and **(C)** fast gamma frequency bands. The black vertical lines indicate the corresponding frequency bands where power matching is performed. The numbers in the legend indicate the subjects obtained after power matching. Solid traces represent the median and shaded region around them indicates $\pm$SEM across subjects, computed after bootstrapping over 10,000 iterations. Coloured bars at the abscissa in the bottom panel represent significance of differences between mid and old (black: $p < 0.05$ and green: $p < 0.01$, K-W test).

HFD provided some additional information than spectral features

To verify further whether HFD provides extra information about the age than those obtained from spectral features, we explored the classifier performance for age distinctiveness using LDA. We used 5 spectral features: alpha power (P_{α}; 8-12 Hz), slow gamma power (P_{SG}; 20-34 Hz), fast gamma power (P_{FG}; 36 to 66 Hz), slope in low frequency range ($Slope_{LFR}$; 64-140 Hz) and slope in high frequency range ($Slope_{HFR}$; 230 to 430 Hz) and 5 similar HFD features: HFD_{α} (1-13 Hz), HFD_{SG} (25-37 Hz), HFD_{FG} (49-61 Hz), HFD_{LFR} (1-90 Hz) and HFD_{HFR} (210-290 Hz). At individual feature level, HFD_{LFR} and $Slope_{LFR}$ performed equally better (AUC = 0.66) among all features. After combining all spectral and HFD features separately, we found AUC slightly higher for all HFD features combined (AUC = 0.71) than all spectral features combined (AUC = 0.69). The spectral features were redundant as compared to HFD features as adding former only improved the AUC to 0.72. These observations suggest that HFD provided some additional information compared to spectral measures and therefore, non-linear techniques may enhance the understanding of brain signals.

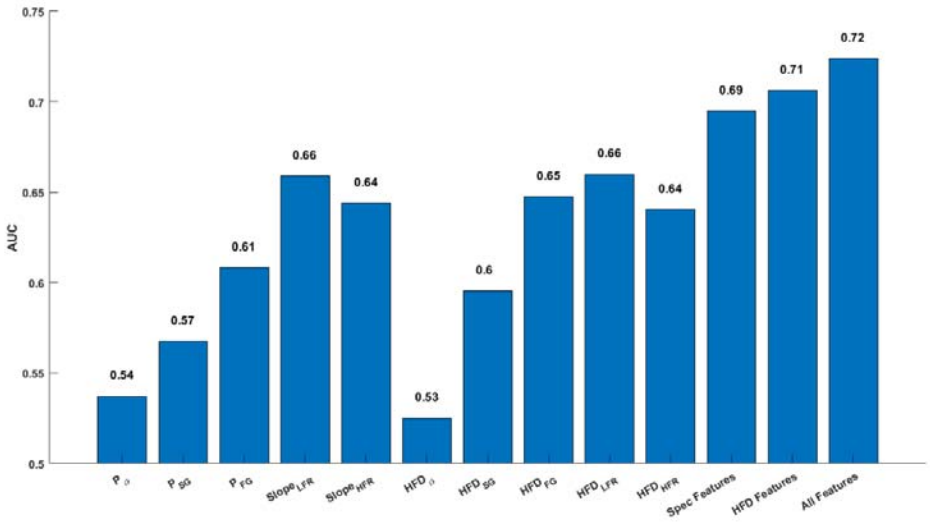

Fig. 7 AUC for different spectral and HFD features individually, all spectral features combined as 'Spec features', all HFD features combined as 'HFD features' and combining all features, computed using 5-fold validation.

Discussion

We investigated dependence of HFD changes on the changes in PSD components (oscillations and the slope of aperiodic activity) by studying the age-related variation of HFD in a high-sampled EEG dataset. The subjects performed a fixation task, where they were shown visual grating stimulus. HFD decreased during the presentation of the stimulus and the reduction was more in mid-aged group (50-65 years) than the old-aged group (>65 years). For BL period, equivalent to eyes open state, HFD increased with age. However, this age-related increase in HFD was limited to frequencies less than 150 Hz and showed opposite trend at higher frequencies. Further, the age-related changes in HFD for the signals, filtered in different frequency range, was negatively related to baseline slope and stimulus-induced oscillatory power in different frequency bands.

We found that presentation of a visual grating stimulus lowered the HFD, which could be due to an increase in the smoothness of the signal (due to the emergence of gamma oscillations) with respect to the spontaneous level. A previous modelling study has shown similar reduction in entropy and complexity due to the stimulus (Ponce-Alvarez et al., 2015). Also, Luczak and colleagues (2009) reported a stimulus-based reduction of multidimensional space outlined by cortical activity. This stimulus-induced decrease in neural variability in terms of reduced firing rate variability has been explained via a spontaneous multi-state stability model (Deco and Hugues, 2012; Litwin-Kumar and Doiron, 2012) and has been linked to information processing. Under the model, the spontaneous activity of local neural networks transits through multiple spontaneous states, thus, rendering it highly heterogeneous (Deco and Hugues, 2012) and has high information capacity (McIntosh et al., 2010). On the other hand, the stimulus stabilizes the network in a single evoked state, resulting in the suppression of the transitions, decrease in variability and enhancement of the transmission of the

information about the stimulus (Ponce-Alvarez et al., 2015). However, stimulus onset also suppresses low-frequency oscillations such as alpha or beta, which can increase HFD. For example, increase in HFD has been reported with respect to sound stimuli (Gladun, 2021). Therefore, there can be an increase or decrease in complexity and HFD with respect to stimulus depending on the frequency range for computation of HFD and the emergence or suppression of oscillations.

The increase in BL HFD with age in the present work seems inconsistent with Smits and colleagues (Smits et al., 2016), who showed an inverse parabola relation of HFD with age between 20-80 years with the decrease in HFD above 50 years. However, as discussed earlier, HFD values are critically dependent on the choice of k_{max}. They chose k_{max} of 65; at low k_{max}, they also found an increase in HFD for older population (fig 2. in (Smits et al., 2016)). Another study also reported an increase in correlation dimension with age, albeit over a different age range of 20-60 years (Anokhin et al., 1996).

The increase in HFD with frequency has also been observed previously but up to 47 Hz only (Ferenets et al., 2007). This is mainly due to increase in roughness or irregularity in signal with increase in its frequency. The different behaviour of age-related variation in HFD in low (<150 Hz) and high frequency ranges (> 150 Hz) indicates the role of frequency range in governing the changes in HFD. Though, the change in HFD was negatively correlated with change in slope (Fig 4C right bottom panel), we did not find a straightforward dependence of HFD on slope (Fig 4C left bottom panel), unlike demonstrated for synthetic signals (Higuchi, 1990) and for colored noise in Fig. 1A. This may be due to our choice of fixing k_{max} to the same value of 5 for all frequency ranges. Also, 1/f slope could be modified due to the presence of oscillations and the intrinsic variation in PSD (Aggarwal and Ray, 2023; Merkin et al., 2023), which could influence the fall of the PSD. Therefore, the negative correlation

became visible only with respect to changes in HFD and slope after the inherent noise cancellation.

Surprisingly, changes in HFD were strongly dependent on the changes in slope rather than the change in broadband power (Fig. 4C right panels), even though, both higher broadband power and shallower slopes at high frequencies are indicators of greater noise in a system. This could be due to different neural mechanisms controlling the origin of broadband power and slopes. For example, while broadband power in high-gamma range is thought to be generated due to increased spiking activity in microelectrode recordings (Ray and Maunsell, 2011), E-I balance is among the widely accepted reasons for the slope modulation (Gao et al., 2017). Though speculative, the dependence of HFD on slope may indicate that HFD could better reflect E-I balance. Moreover, E-I balance plays an important role in the generation of stimulus-induced oscillatory gamma power (Wilson and Cowan, 1972; Fuchs et al., 2007; Buzsáki and Wang, 2012). Thus, the negative dependence of HFD on stimulus-induced gamma power (Fig. 6) provides further hints for the existence of a relation between HFD and E-I balance. Future studies can help shed light on more reasons for the dependence of HFD on slope and stimulus-induced gamma power but not overall broadband power.

We found conflicting description about the correlation between HFD and power in different frequency bands in literature. This could be because power in a given frequency band may increase due to an oscillation in that frequency range (bump in the PSD) or an increase in broadband power which leads to an increase in the “pedestal” of the PSD, even though these two types of change (narrowband versus broadband) may have opposite effects on HFD. For example, HFD has been shown to decrease in chronic insomniacs compared to controls, which was related to increased alpha power, mainly in the right hemisphere, in patients with insomnia (Kronholm et al., 2007). Further, HFD has been correlated negatively with theta

activity but positively with gamma activity (Stojadinović et al., 2020). Along with direct comparisons, indirect correlations may be inferred by comparing HFD and power-based studies. For example, in depression, both HFD (Akar et al., 2015) and power (Strelets et al., 2007) in gamma band increases, indicating a positive correlation. Similarly, reduced HFD in AD (Smits et al., 2016) and increased gamma power during resting state (van Deursen et al., 2008; Güntekin et al., 2020; Fide et al., 2021) hint at a negative correlation. P□eske and colleagues surveyed several studies and found HFD to be negatively correlated with theta, alpha and beta band power but weakly positively related to gamma band power (Päeske et al., 2023). However, most of these studies involved resting state brain activity (Kronholm et al., 2007; Smits et al., 2016; Stojadinović et al., 2020), that is dominated by low frequency peak oscillations, so their high frequency activity may not be oscillatory. Also, in these studies, HFD computed for broadband frequency ranges were correlated with narrow band oscillations, while we computed HFD and power in the same frequency bands. An important point is that during the BL period in the present study (Fig. 4), the old-aged group has flatter PSD and corresponding higher power above 50 Hz. If we consider power in gamma range (30-80 Hz), our results would also indicate that increase in HFD is related to increase in gamma power. So, one needs to be cautious about the oscillatory power that are characterised by peaks in the PSD spectrum and the broadband power that can be indicative of slopes.

Classification studies provide mixed results about the performance comparison between HFD and band power. While HFD and band power performed equally for the classification of schizophrenic patients (Sabeti et al., 2007) and depressive state using LDA classifier (Hosseinifard et al., 2013), HFD showed slightly higher accuracy (3.3%) over alpha band power for the latter classification when a different classification technique (logistic regression) was used (Hosseinifard et al., 2013). These results indicate a strong dependence of HFD on power similar to the present work where HFD performed slightly better than

power measures. However, the improvement of AUC using HFD by ~0.02 (2%; AUC_{HFD} = 0.71 and AUC_{Spec} = 0.69) hints at a slight advantage of nonlinear methods over linear methods for classification.

The present work highlights that one needs to be cautious while drawing conclusions from the changes in HFD as these changes could be dominated by changes in traditional spectral measures. Interestingly, the dependence of HFD on spectral measures (oscillations and slope) could help in predicting the directional change of the other measure, if one of them is known. Further, it could lead to better models to explain brain dynamics including both spectral parameters and HFD, than separate models based on them.

References

Accardo A, Affinito M, Carrozzi M, Bouquet F (1997) Use of the fractal dimension for the analysis of electroencephalographic time series. Biol Cybern 77:339–350.

Aggarwal S, Ray S (2023) Slope of the power spectral density flattens at low frequencies (<150 Hz) with healthy aging but also steepens at higher frequency (>200 Hz) in human electroencephalogram. Cerebral Cortex Communications 4:tgad011.

Akar SA, Kara S, Agambayev S, Bilgic V (2015) Nonlinear analysis of EEG in major depression with fractal dimensions. Annu Int Conf IEEE Eng Med Biol Soc 2015:7410–7413.

Amezquita-Sanchez JP, Mammone N, Morabito FC, Marino S, Adeli H (2019) A novel methodology for automated differential diagnosis of mild cognitive impairment and the Alzheimer's disease using EEG signals. Journal of Neuroscience Methods 322:88–95.

Anokhin AP, Birbaumer N, Lutzenberger W, Nikolaev A, Vogel F (1996) Age increases brain complexity. Electroencephalography and Clinical Neurophysiology 99:63–68.

Babiloni C, Binetti G, Cassarino A, Dal Forno G, Del Percio C, Ferreri F, Ferri R, Frisoni G, Galderisi S, Hirata K, Lanuzza B, Miniussi C, Mucci A, Nobili F, Rodriguez G, sLuca Romani G, Rossini PM (2006) Sources of cortical rhythms in adults during physiological aging: a multicentric EEG study. Hum Brain Mapp 27:162–172.

Barabási A-L, Vicsek T (1991) Multifractality of self-affine fractals. Phys Rev A 44:2730–2733.

Bokil H, Andrews P, Kulkarni JE, Mehta S, Mitra PP (2010) Chronux: a platform for analyzing neural signals. J Neurosci Methods 192:146–151.

Buzsáki G, Wang X-J (2012) Mechanisms of Gamma Oscillations. Annu Rev Neurosci 35:203–225.

Churchland MM et al. (2010) Stimulus onset quenches neural variability: a widespread cortical phenomenon. Nat Neurosci 13:369–378.

Deco G, Hugues E (2012) Neural Network Mechanisms Underlying Stimulus Driven Variability Reduction. PLOS Computational Biology 8:e1002395.

Delorme A, Makeig S (2004) EEGLAB: an open source toolbox for analysis of single-trial EEG dynamics including independent component analysis. J Neurosci Methods 134:9–21.

Díaz Beltrán L, Madan CR, Finke C, Krohn S, Di Ieva A, Esteban FJ (2024) Fractal Dimension Analysis in Neurological Disorders: An Overview. In: The Fractal Geometry of the Brain (Di Ieva A, ed), pp 313–328. Cham: Springer International Publishing. Available at: https://doi.org/10.1007/978-3-031-47606-8_16 [Accessed May 6, 2024].

Donoghue T, Haller M, Peterson EJ, Varma P, Sebastian P, Gao R, Noto T, Lara AH, Wallis JD, Knight RT, Shestyuk A, Voytek B (2020) Parameterizing neural power spectra into periodic and aperiodic components. Nat Neurosci 23:1655–1665.

Drachman DA (2006) Aging of the brain, entropy, and Alzheimer disease. Neurology 67:1340–1352.

720 Eke A, Hermán P, Bassingthwaighte J, Raymond G, Percival D, Cannon M, Balla I, Ikrényi C (2000)
721 Physiological time series: distinguishing fractal noises from motions. Pflügers Arch – Eur J
722 Physiol 439:403–415.

723 Esteller R, Vachtsevanos G, Echauz J, Litt B (2001) A comparison of waveform fractal dimension
724 algorithms. IEEE Trans Circuits Syst I 48:177–183.

725 Falconer K (2013) Fractal Geometry: Mathematical Foundations and Applications. John Wiley & Sons.

726 Ferenets R, Vanluchene A, Lipping T, Heyse B, Struys MMRF (2007) Behavior of entropy/complexity
727 measures of the electroencephalogram during propofol-induced sedation: dose-dependent
728 effects of remifentanil. Anesthesiology 106:696–706.

729 Fide E, Yerlikaya D, Yener G (2021) Resting-state EEG gamma power and coherence might be an
730 indicator of hyperexitability in patients with early-onset Alzheimer's disease. Alzheimer's &
731 Dementia 17:e058669.

732 Fuchs EC, Zivkovic AR, Cunningham MO, Middleton S, LeBeau FEN, Bannerman DM, Rozov A,
733 Whittington MA, Traub RD, Rawlins JNP, Monyer H (2007) Recruitment of Parvalbumin-
734 Positive Interneurons Determines Hippocampal Function and Associated Behavior. Neuron
735 53:591–604.

736 Gao R, Peterson EJ, Voytek B (2017) Inferring synaptic excitation/inhibition balance from field
737 potentials. NeuroImage 158:70–78.

738 Gladun KV (2021) Higuchi Fractal Dimension as a Method for Assessing Response to Sound Stimuli in
739 Patients with Diffuse Axonal Brain Injury. Sovrem Tekhnologii Med 12:63–70.

740 Güntekin B, Yıldırım E, Kıyı İ, Fide E, Uzunlar H, Calısoglu P, Yirikogullari H, Akturk T, Yener G (2020)
741 Gamma power increased in Alzheimer's disease patients in comparison to healthy controls
742 during recognition of facial expressions. Alzheimer's & Dementia 16:e043387.

743 Harada CN, Natelson Love MC, Triebel KL (2013) Normal Cognitive Aging. Clinics in Geriatric
744 Medicine 29:737–752.

745 Higuchi T (1988) Approach to an irregular time series on the basis of the fractal theory. Physica D:
746 Nonlinear Phenomena 31:277–283.

747 Higuchi T (1990) Relationship between the fractal dimension and the power law index for a time
748 series: A numerical investigation. Physica D: Nonlinear Phenomena 46:254–264.

749 Hogan MJ, Kilmartin L, Keane M, Collins P, Staff RT, Kaiser J, Lai R, Upton N (2012)
750 Electrophysiological entropy in younger adults, older controls and older cognitively declined
751 adults. Brain Research 1445:1–10.

752 Hosseinifard B, Moradi MH, Rostami R (2013) Classifying depression patients and normal subjects
753 using machine learning techniques and nonlinear features from EEG signal. Computer
754 Methods and Programs in Biomedicine 109:339–345.

755 Kesić S, Spasić SZ (2016) Application of Higuchi's fractal dimension from basic to clinical
756 neurophysiology: A review. Computer Methods and Programs in Biomedicine 133:55–70.

Kronholm E, Virkkala J, Kärki T, Karjalainen P, Lang H, Hämäläinen H (2007) Spectral power and fractal dimension: Methodological comparison in a sample of normal sleepers and chronic insomniacs. Sleep Biol Rhythms 5:239–250.

Kumar WS, Manikandan K, Murty DVPS, Ramesh RG, Purokayastha S, Javali M, Rao NP, Ray S (2022) Stimulus-Induced Narrowband Gamma Oscillations are Test–Retest Reliable in Human EEG. Cereb Cortex Commun 3:tgab066.

Kumar WS, Ray S (2023) Healthy ageing and cognitive impairment alter EEG functional connectivity in distinct frequency bands. European Journal of Neuroscience 58:3432–3449.

Lau ZJ, Pham T, Chen SHA, Makowski D (2022) Brain entropy, fractal dimensions and predictability: A review of complexity measures for EEG in healthy and neuropsychiatric populations. European Journal of Neuroscience 56:5047–5069.

Litwin-Kumar A, Doiron B (2012) Slow dynamics and high variability in balanced cortical networks with clustered connections. Nat Neurosci 15:1498–1505.

Luczak A, Barthó P, Harris KD (2009) Spontaneous Events Outline the Realm of Possible Sensory Responses in Neocortical Populations. Neuron 62:413–425.

Mandelbrot BB (1985) Self-Affine Fractals and Fractal Dimension. Phys Scr 32:257.

Mandelbrot BB (2013) Fractals and Scaling in Finance: Discontinuity, Concentration, Risk. Selecta Volume E. Springer Science & Business Media.

Mandelbrot BB, Van Ness JW (1968) Fractional Brownian Motions, Fractional Noises and Applications. SIAM Rev 10:422–437.

Matteo TD, Aste T, Dacorogna MM (2005) Long-term memories of developed and emerging markets: Using the scaling analysis to characterize their stage of development. Journal of Banking & Finance 29:827–851.

McIntosh AR, Vakorin V, Kovacevic N, Wang H, Diaconescu A, Protzner AB (2014) Spatiotemporal Dependency of Age-Related Changes in Brain Signal Variability. Cerebral Cortex 24:1806–1817.

Merkin A, Sghirripa S, Graetz L, Smith AE, Hordacre B, Harris R, Pitcher J, Semmler J, Rogasch NC, Goldsworthy M (2023) Do age-related differences in aperiodic neural activity explain differences in resting EEG alpha? Neurobiology of Aging 121:78–87.

Molz FJ, Liu HH, Szulga J (1997) Fractional Brownian motion and fractional Gaussian noise in subsurface hydrology: A review, presentation of fundamental properties, and extensions. Water Resources Research 33:2273–2286.

Morel P (2018) Gramm: grammar of graphics plotting in Matlab. Journal of Open Source Software 3:568.

Murty DV, Manikandan K, Kumar WS, Ramesh RG, Purokayastha S, Nagendra B, ML A, Balakrishnan A, Javali M, Rao NP, Ray S (2021) Stimulus-induced gamma rhythms are weaker in human elderly with mild cognitive impairment and Alzheimer's disease Vinck M, Colgin LL, Bosman CA, eds. eLife 10:e61666.

Murty DVPS, Manikandan K, Kumar WS, Ramesh RG, Purokayastha S, Javali M, Rao NP, Ray S (2020) Gamma oscillations weaken with age in healthy elderly in human EEG. NeuroImage 215:116826.

Murty DVPS, Ray S (2022) Stimulus-induced Robust Narrow-band Gamma Oscillations in Human EEG Using Cartesian Gratings. Bio Protoc 12:e4379.

Olejarczyk E, Cukic M, Porcaro C, Zappasodi F, Tecchio F (2024) Clinical Sensitivity of Fractal Neurodynamics. In: The Fractal Geometry of the Brain (Di Ieva A, ed), pp 285–312. Cham: Springer International Publishing.

Orey S (1970) Gaussian sample functions and the Hausdorff dimension of level crossings. Z Wahrscheinlichkeitstheorie verw Gebiete 15:249–256.

Päeske L, Uudeberg T, Hinrikus H, Lass J, Bachmann M (2023) Correlation between electroencephalographic markers in the healthy brain. Sci Rep 13:6307.

Phillips LH, Andrés P (2010) The cognitive neuroscience of aging: new findings on compensation and connectivity. Cortex; a Journal Devoted to the Study of the Nervous System and Behavior 46:421–424.

Ponce-Alvarez A, He BJ, Hagmann P, Deco G (2015) Task-Driven Activity Reduces the Cortical Activity Space of the Brain: Experiment and Whole-Brain Modeling. PLOS Computational Biology 11:e1004445.

Rabinovich MI, Varona P, Selverston AI, Abarbanel HDI (2006) Dynamical principles in neuroscience. Rev Mod Phys 78:1213–1265.

Raghavendra BS, Dutt DN (2011) Nonlinear Dynamical Characterization of Heart Rate Variability Time Series of Meditation. International Journal of Biomedical and Biological Engineering 5:429–440.

Ray S, Maunsell JHR (2011) Different Origins of Gamma Rhythm and High-Gamma Activity in Macaque Visual Cortex. PLOS Biology 9:e1000610.

Sabeti M, Boostani R, Katebi SD, Price GW (2007) Selection of relevant features for EEG signal classification of schizophrenic patients. Biomedical Signal Processing and Control 2:122–134.

Scally B, Burke MR, Bunce D, Delvenne J-F (2018) Resting-state EEG power and connectivity are associated with alpha peak frequency slowing in healthy aging. Neurobiol Aging 71:149–155.

Smits FM, Porcaro C, Cottone C, Cancelli A, Rossini PM, Tecchio F (2016) Electroencephalographic Fractal Dimension in Healthy Ageing and Alzheimer's Disease. PLOS ONE 11:e0149587.

Spasić S, Kalauzi A, Ćulić M, Grbić G, Martać L (2005) Estimation of Parameter kmax in Fractal Analysis of Rat Brain Activity. Annals of the New York Academy of Sciences 1048:427–429.

Stojadinović G, Martać L, Podgorac J, Spasić SZ, Petković B, Sekulić S, Kesić S (2020) The effects of Nembutal on the intracerebellar EEG activity revealed by spectral and fractal analysis. Archives of Biological Sciences 72:425–432.

Strelets VB, Garakh ZhV, Novototskii-Vlasov VYu (2007) Comparative study of the gamma rhythm in normal conditions, during examination stress, and in patients with first depressive episode. Neurosci Behav Physiol 37:387–394.

van Deursen JA, Vuurman EFPM, Verhey FRJ, van Kranen-Mastenbroek VHJM, Riedel WJ (2008) Increased EEG gamma band activity in Alzheimer's disease and mild cognitive impairment. J Neural Transm (Vienna) 115:1301–1311.

Voytek B, Kramer MA, Case J, Lepage KQ, Tempesta ZR, Knight RT, Gazzaley A (2015) Age-Related Changes in 1/f Neural Electrophysiological Noise. Journal of Neuroscience 35:13257–13265.

Werner G (2010) Fractals in the Nervous System: Conceptual Implications for Theoretical Neuroscience. Front Physiol 1:15.

Wilson HR, Cowan JD (1972) Excitatory and Inhibitory Interactions in Localized Populations of Model Neurons. Biophysical Journal 12:1–24.

Supplementary Material

Computation of H

We used generalised Hurst exponent method to compute H, that involves the qth order moments $K_q(r)$ of the distribution of the increments (Barabási and Vicsek, 1991; Matteo et al., 2005; Mandelbrot, 2013).

$K_q(r)$ for the time series $X(1), X(2), X(3), \ldots, X(N)$, is given by

$$K_q(r) = \frac{< |X(t+r) - X(t)|^q >}{< |X(t)|^q >}$$

where *r* varies from 1 to r_{max} (*r* plays a similar role for calculating H as *k* in HFD). $K_q(r)$ is assumed to follow the relation

$$K_q(r) \sim r^{qH(q)}$$

where *H(q)* is the generalised H.

We used the matlab code (https://in.mathworks.com/matlabcentral/fileexchange/30076-generalized-hurst-exponent) to calculate H for first order moments with the default parameters, $q = 1$ and $r_{\max}$ =19.

We found a close match between theoretical result of FD = 2-H and the observed results, where HFD+H =1.985$\pm$0.001, computed for the experimental data.

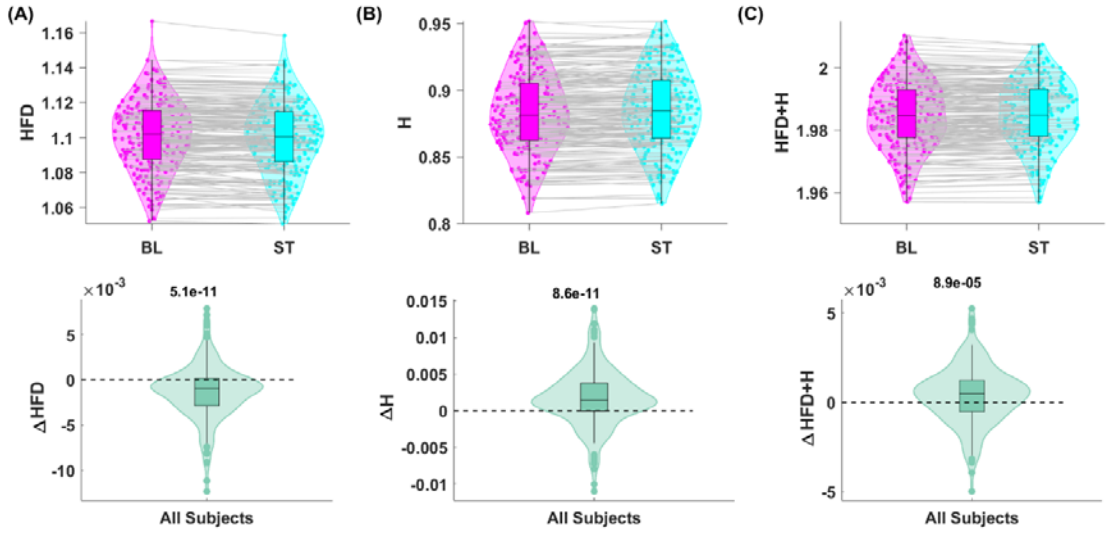

Supplementary Fig. 1 Violin plots showing the distribution of **(A)** HFD, **(B)** H and **(C)** HFD+H for BL and ST (top panel) and their difference (bottom panel) for all subjects (N=217). p-values obtained from Wilcoxon signed rank test are indicated at the top of the bottom panels.